MAGNETIC RESONANCE IN CHEMISTRY, VOL. 30, 1178–1185 (1992)

NMR Studies of Hindered Rotation and Thermal Decomposition of Novel 1-Aryl-3,3-dialkyltriazenes

Th. Lippert and A. Wokaun*
Department of Physical Chemistry II, University of Bayreuth, D-W-8580 Bayreuth, Germany

J. Dauth† and O. Nuyken
Department of Macromolecular Chemistry I, University of Bayreuth, D-W-8580 Bayreuth, Germany

1-Aryl-3,3-dialkyltriazenes have been synthesized by coupling the corresponding diazonium salts of substituted aniline derivatives with dialkylamines. The thermostability of these compounds was investigated by differential scanning calorimetry; activation energies of 240–280 kJ mol^{-1} were determined for the thermal decomposition. The hindered rotation of the dialkylamino group was studied by ^{1}H NMR exchange measurements. Both experiments are interpreted in terms of an involvement of a 1,3-dipolar structure of the —N=N—N— functional group. The influence of substituents, both on the aromatic ring and at the amino group, on the kinetic and activation parameters is investigated; results are analysed on the basis of mesomeric and steric effects on the dipolar charge distribution in the molecule.

KEY WORDS 1-Aryl-3,3-dialkyltriazenes ^{1}H NMR Hindered rotation Thermal decomposition

INTRODUCTION

Triazenes of the general structure

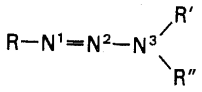

which contain the characteristic N=N—N functional group, were first synthesized in 1903.[1] These compounds (with R = phenyl) are unstable in acids, and decompose[2,3] into substituted anilines (R″ = H), benzene derivatives and nitrogen. Furthermore, triazenes can be photolysed by UV illumination with release of nitrogen.[4] This photolability, as well as the discovery of antitumour activity for certain derivatives,[5] have been the reasons for the recent interest in this class of compounds. In particular, the effect of 1-aryl-3,3-dialkyltriazenes as antitumour reagents has been studied in some detail.[5] However, to our knowledge, the thermal decomposition behaviour has not been investigated.

Akthar *et al.*[6] have proposed that the π electron distribution in triazenes partly corresponds to the 1,3-dipolar resonance structure (**II**) shown in Scheme 1.

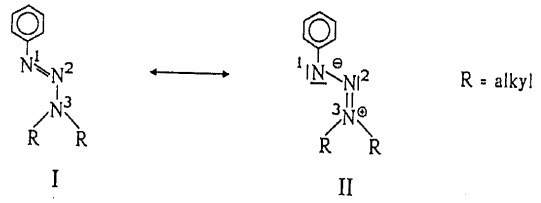

Scheme 1

The result of such a resonance hybridization is an increase in the effective rotation barrier around the N^2—N^3 single bond. In this study, rotation barriers for a series of differently substituted triazenes were determined by NMR techniques. The influence of the substituents on the thermal stability of the triazenes was investigated by differential scanning calorimetry (DSC) measurements.

The triazenes were prepared according to Scheme 2.

Six compounds have been synthesized which differ in their substituents (R_1 to R_4), as specified in Table 1.

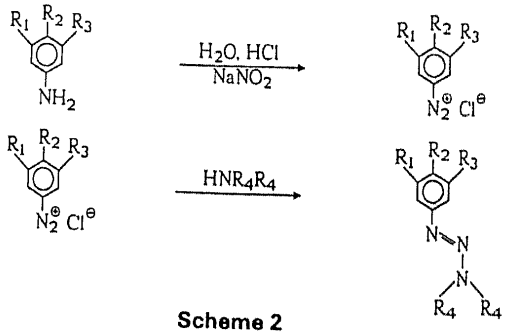

Scheme 2

* Author to whom correspondence should be addressed.
† Present address: Wacker Chemie GmbH, Werk Burghausen, Johannes Hess-Strasse 24, D-W-8263 Burghausen, Germany.

0749–1581/92/121178–08 $09.00

Received 28 February 1992
Accepted (revised) 30 June 1992

Table 1. Substituted triazene compounds investigated in this study

Compund	R_1	R_2	R_3	R_4[a]	$\Delta\nu$ (Hz)[b]
1	H	H	COOH	C_2H_5	36.2
2	H	H	COOH	n-C_3H_7	27.0[c]
3	H	H	COOH	i-C_3H_7	40.9
4	COOH	H	COOH	C_2H_5	36.2
5	H	COOH	H	C_2H_5	38.1
6	H	CN	H	C_2H_5	39.6

[a] Positions of the substituents $R_1, \ldots, R_4$ are shown in Scheme 2.
[b] Chemical shift difference of the two CH_3 groups in the R_4 substituents.
[c] Chemical shift difference of the two $N-CH_2$ groups.

EXPERIMENTAL

Reagents

Aniline derivatives and amines were obtained from Aldrich and Fluka in the highest available purities (99%). All solvents were freshly distilled before use. Syntheses were carried out in the dark.

General synthesis procedure (LeBlanc and Vaughan[7])

Diazotization. The appropriate aromatic amine (1×10^{-2} mol) was dissolved in 30 ml of aqueous hydrochloric acid solution (10%) and cooled to $-10\,^{\circ}C$. A solution of 1×10^{-2} mol sodium nitrite in 20 ml of water was then added slowly with vigorous stirring. The reaction temperature was kept below $-5\,^{\circ}C$. The mixture was stirred for a further 15 minutes and was used in the following step without separation of the corresponding diazonium salt.

Coupling with dialkylamines. An aqueous, precooled solution of the dialkylamine (2×10^{-2} mol, i.e. a twofold stoichiometric excess) was added to the freshly prepared diazonium salt solution. The temperature was kept below $0\,^{\circ}C$ throughout the entire time of reaction. An intense yellow colour appeared, and the triazene product precipitated immediately. The product was filtered off, washed with water and dried over phosphorous pentoxide. The products were recrystallized in either methanol or methanol–water mixtures. The characterization data of all products are compiled in the Appendix.

Synthesis of 1-(3-carboxyphenyl)-3,3-diethyltriazene (1)

Diazotization of 1×10^{-2} mol of 3-aminobenzoic acid and coupling of the corresponding diazonium salt with diethylamine were carried out according to the general synthesis procedure. The product dissolved on deprotonation of the carboxylic acid groups during addition of the amine in stoichiometric excess. The triazene was reprecipitated by adjusting the pH to a value of 5 by the addition of a 0.1 M aqueous hydrochloric acid solution. The yield was 1.4 g, i.e. 63% based on the amount of the 3-aminobenzoic acid reactant.

Synthesis of 1-(3-carboxyphenyl)-3,3-di-n-propyltriazene (2)

Diazotization of 1×10^{-2} mol of 3-aminobenzoic acid, the coupling reaction with di-*n*-propylamine and the purification procedure were carried out as described for compound **1**. The yield was 1.7 g (67% based on the 3-aminobenzoic acid reactant).

Synthesis of 1-(3-carboxyphenyl)-3,3-diisopropyltriazene (3)

Diazotization of 1×10^{-2} mol of 3-aminobenzoic acid, coupling with diisopropylamine and purification were performed as described for compound **1**. The yield was 1.9 g (76% based on the 3-aminobenzoic acid reactant).

Synthesis of 1-(3,5-dicarboxyphenyl)-3,3-diethyltriazene (4)

Diazotization of 1×10^{-2} mol of 5-aminoisophthalic acid and the coupling with diethylamine were carried out according to the general synthesis procedure. As a consequence of the insolubility of the aniline derivative in water, the suspension had to be stirred for 30 minutes until diazotization was complete. After addition of diethylamine in excess, the product was purified as described for compound **1**. The yield was 1.1 g (34% based on the 5-aminoisophthalic acid reactant).

Synthesis of 1-(4-carboxyphenyl)-3,3-diethyltriazene (5)

Diazotization of 1×10^{-2} mol of 4-aminobenzoic acid, coupling with diethylamine and purification were performed as described for compound **1**. The yield was 1.7 g (76% based on the 4-aminobenzoic acid reactant).

Synthesis of 1-(4-cyanophenyl)-3,3-diethyltriazene (6)

Diazotization of 4-aminobenzoic acid nitrile and the coupling of the corresponding diazonium salt solution with diethylamine were carried out according to the general synthesis procedure. The yield was 1.6 g (81% based on the 4-aminobenzoic acid nitrile reactant).

Instruments

NMR measurements were performed on 250 MHz (Bruker, Model AC 250) and on 300 MHz (Bruker, Model AC 300) spectrometers. The temperature was controlled by a variable temperature unit (Bruker, Model B VT 1000). Thermal analysis runs were carried out on a differential scanning calorimeter (Perkin-Elmer, Model DSC 7) using a temperature scan rate of 10 K/min. Infra-red spectra were recorded on a Fourier transform instrument (Digilab, Model FTS-40). Elemental analyses were performed at the Analytisches Laboratorium Ilse Beltz, D-W-8640 Kronach.

RESULTS

NMR observation of intramolecular rotation

NMR spectra of compounds **1–6** were recorded on the 300 MHz NMR spectrometer for a series of temperatures. Coalescence temperatures were determined for the signals of the methyl protons for compounds **1** and **3–6**. The chemical shift difference of the methyl groups in **2** is too small to derive the kinetic parameters; the methylene groups attached to nitrogen were therefore used for the determination of coalescence.

At low temperatures the relevant signals of compounds **1**, **2** and **4–6** show two triplets of equal intensity, which broaden at higher temperatures. Above the coalescence temperature the signals change to a single triplet, as shown in Fig. 1. Two doublets are observed for the methyl groups of the *i*-C_3H_7 substituents in **3**. The large difference in chemical shifts (4.15 and 5.35 ppm, $\Delta\nu = 358$ Hz at 263 K) for the signals of the two non-equivalent *i*-C_3H_7 methine protons might be due to the involvement of the ionic resonance structure **II** in Scheme 1. As a consequence of the hindered rotation, the two isopropyl groups have *Z* and *E* geometries with respect to the aniline moiety.

The temperature dependence of the exchange rate was examined by the line width method[8] both above and below the coalescence temperature. Vaues for $\Delta G^{\neq}$, $\Delta H^{\neq}$, $\Delta S^{\neq}$, and the activation energy, E_a, of the hindered internal rotation, which exchanges the two R_4 substituents, have been determined from standard equations, which were used in the form given by Anderson and Lehn[8] adapted for linear regression analysis.

$$\Delta G^{\neq} = 2.3RT\left(10.32 + \log\frac{T}{k}\right) \quad (1)$$

$$\log\frac{k}{T} = 10.32 + \frac{\Delta S^{\neq}}{2.3R} - \frac{\Delta H^{\neq}}{2.3RT} \quad (2)$$

$$\log k = C - \frac{E_a}{2.3RT} \quad (3)$$

In these equations k is the rate constant (in s^{-1}) of substituent exchange by internal rotation, C is the logarithm of the corresponding frequency factor and T is the temperature in K. The free energy $\Delta G^{\neq}$, enthalpy $\Delta H^{\neq}$ and energy of activation, E_a, for the internal rotation process are given in kJ mol^{-1}, and the activation entropy, $\Delta S^{\neq}$, in J mol^{-1} K^{-1}.

As an example, a typical plot of experimental data for the calculation of $\Delta H^{\neq}$ and $\Delta S^{\neq}$ according to Eqn (2) is shown in Fig. 2. The entire set of kinetic parameters derived from least-squares linear regression analysis is summarized in Table 2.

Thermoanalytical measurements

Thermolysis of the synthesized triazene derivatives was carried out in the solid state by DSC measurements. A typical DSC curve for compound **2** is shown in Fig. 3. An endothermic melting peak at 84 °C is followed by a broad exothermic decomposition event at ≈120 °C.

Rate constants and activation energies for thermal decomposition have been determined from the DSC curves using the analysis for first-order kinetics. This assumption is suggested by the structural similarity of the thermolabile triazene group with aryl-alkyl-azo compounds.[9,10] The procedure used for the determination of the temperature-dependent rate constants $k(T)$ is illustrated using the example of the DSC curve shown in Fig. 4. In the DSC instrument, the heat flow dH/dt [W] is measured as a function of time. Temperature is simply related to the time axis by the linear temperature program

$$T(t) = T(0) + \alpha t \quad (4)$$

where α is the scan rate in K s^{-1}. The total area A [J] of the DSC curve is proportional to the initial amount of material, $n(0)$ [mol]

$$n(0) = CA \quad (5)$$

Similarly, the undecomposed number of moles at time t, $n(t)$, is given by (cf. Fig. 4)

$$n(t) = C(A - a) \quad (6)$$

and the rate of decrease is proportional to the instantaneous heat flow

$$\frac{dn(t)}{dt} = C\frac{dH}{dt} \quad \left(\frac{dH}{dt} < 0\right) \quad (7)$$

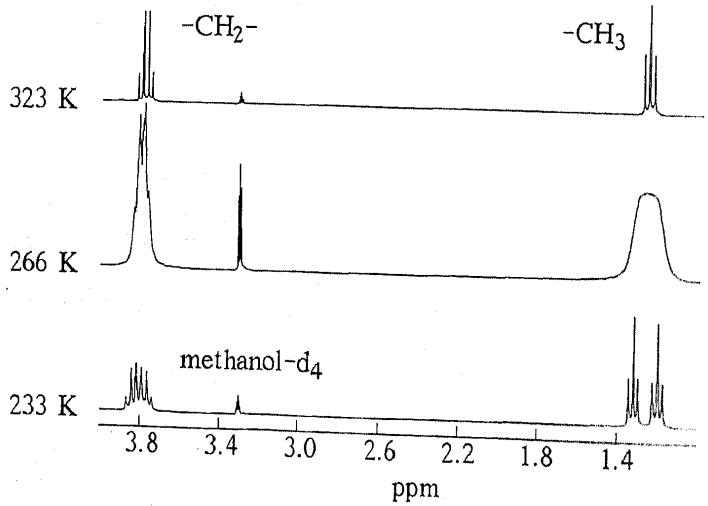

Figure 1. NMR spectra of compound **1**, recorded at 300 MHz in methanol-d_4 at the temperatures indicated.

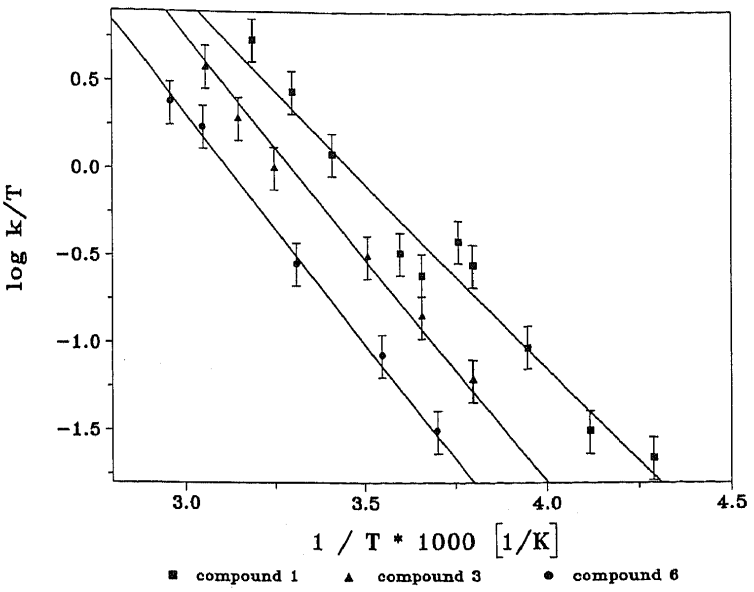

Figure 2. Determination of the activation enthalpies and entropies for internal rotation, $\Delta H^{\neq}$ and $\Delta S^{\neq}$, according to Eqn (2). The quantity $\log[k(T)/T]$, determined from NMR measurements of the temperature-dependent exchange rate $k(T)$ in methanol-d_4, is plotted as a function of $1/T$ for compounds **1**, **3** and **6**.

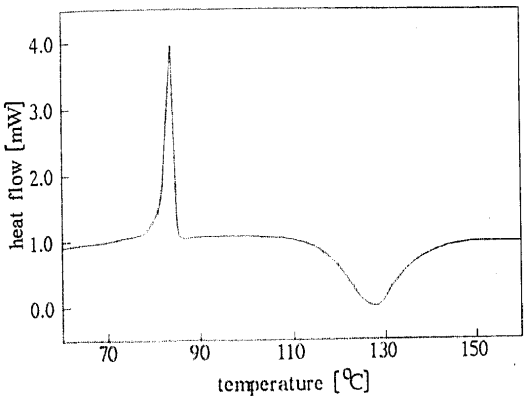

Figure 3. Thermal decomposition of triazene **2** monitored by differential scanning calorimetry.

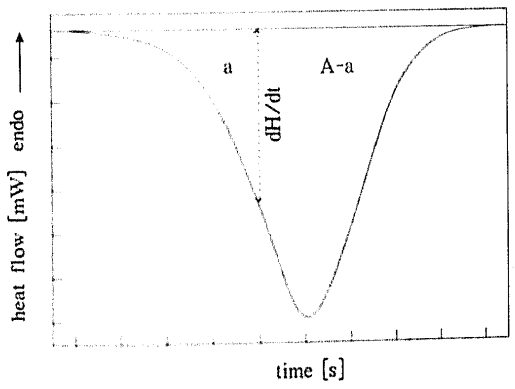

Figure 4. Determination of the temperature dependent decomposition rate constant $k(T)$ from the differential scanning calorimetry curve, according to Eqn (9).

From the standard first-order kinetic equation

$$\frac{dn(t)}{dt} = -k(T)n(t) \tag{8}$$

one obtains

$$k(T) = \frac{1}{A-a}\left|\frac{dH}{dt}\right| \tag{9}$$

This analysis is valid as long as

$$\frac{1}{k(T_{max})} \ll \frac{1}{\alpha}(T_{max} - T_{min}) \ll \frac{1}{k(T_{min})} \tag{10}$$

In this equation, T_{min} and T_{max} signify the initial and final temperature of the decomposition peak, defined as the temperatures where $|dH/dt|$ has decreased to 10% of its peak value. The quantity $[1/\alpha(T_{max} - T_{min})]$ is the time required to scan over the peak. This time should be much shorter than the half-life of the reaction, $[1/k(T_{min})]$, at the peak onset, and longer than the half-life $[1/k(T_{max})]$ at the end of the peak.

An Arrhenius plot for **4** derived from three independent measurements is shown in Fig. 5. The activation energies of thermal decomposition for the triazene derivatives **2**, **4** and **5** derived from the DSC data are summarized in Table 3.

It was not possible to calculate A and E_a for **3** because of the overlap of the melting and decomposition peaks. Compound **6** sublimes before decomposition, with the result that again the parameters of thermal decay could not be determined.

Table 2. Activation parameters and coalescence temperatures derived from NMR analysis

Compound	T_c (K)	$\Delta G^{\neq}$ (kJ mol^{-1})	$\Delta H^{\neq}$ (kJ mol^{-1})	$\Delta S^{\neq}$ (J mol^{-1} K^{-1})	E_a (kJ mol^{-1})	$C = \log A/s^{-1}$
1	266 ± 0.5	57.5 ± 2.9 at 293 K	40.5 ± 2.9	−57.0 ± 11.5	45.8 ± 1.8	11.0 ± 0.03
2	274 ± 0.5	56.9 ± 2.9 at 268 K	31.3 ± 3.9	−95.2 ± 14.1	37.7 ± 2.1	9.1 ± 0.02
3	285 ± 0.5	58.6 ± 2.9 at 273 K	48.9 ± 3.0	−36.0 ± 10.2	53.4 ± 1.8	12.0 ± 0.03
4	280 ± 0.5	58.3 ± 2.9 at 280 K	41.1 ± 4.9	−60.0 ± 18.0	47.7 ± 2.9	11.0 ± 0.04
5	283 ± 0.5	61.4 ± 3.1 at 310 K	50.5 ± 10.9	−34.7 ± 10.6	45.8 ± 4.6	10.0 ± 0.06
6	302 ± 0.5	62.8 ± 3.1 at 302 K	50.5 ± 3.8	−39.9 ± 12.7	53.4 ± 1.1	11.0 ± 0.02

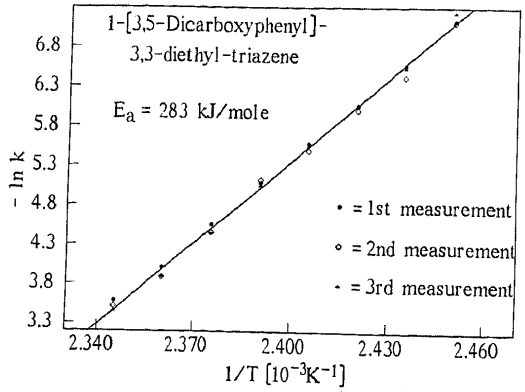

Figure 5. Arrhenius plot for the decomposition of compound **4**.

Table 3. Thermal decomposition parameters of compounds 1–6 derived from DSC measurements

Compound	T_{max} [a] (°C)	E_a (kJ mol^{-1})	ln A/s^{-1}
1	113	282 ± 10	−84 ± 0.02
2	128	221 ± 8	−62 ± 0.04
3	136	[b]	
4	151	282 ± 3	−76 ± 0.01
5	148	242 ± 12	−66 ± 0.02
6	[c]	[c]	

[a] T_{max} = temperature of maximum heat flow $|dH/dt|$.
[b] Not measurable because of the overlap with the melting peak.
[c] Sublimation before decomposition.

DISCUSSION

Both the hindered rotation around the $N^2—N^3$ bond, as monitored in the NMR measurements, and the thermal decomposition determined by DSC are strongly influenced by the electronic structure and the charge distribution in the triazene functional group. We have indicated earlier that the charge distribution in the $N^1=N^2—N^3$ fragment corresponds to a 1,3-dipolar structure, with a partial negative charge on N^1, due to a contribution from the mesomeric resonance structure **II** shown in Scheme 1.

The possibility of a further delocalization of this negative charge from N^1 on to the phenyl ring can be considered, which would give rise to a *para*-quinonoid type structure. The importance of such a shift of charge can be judged from the spectral pattern of the aromatic protons. For a quinonoid limiting structure a hindered rotation around the phenyl—N^1 bond would be expected, and hence an AB XY type spectrum for the *para*-substituted compounds ($R_1 = R_3 = H$). However, clean spectra corresponding to AA′XX′ spin systems were recorded, which indicates rapid rotation around the phenyl—N^1 bond. Hence charge delocalization on to the aromic ring appears not to be important.

However, the amount of shifted charge, as related to the 1,3-dipolar structure, is expected to be strongly influenced by mesomeric effects due to substituents on the phenyl ring, and by inductive and steric effects due to the alkyl substituents on the nitrogen atom N^3.

Among the substituents in the compounds studied (Table 1), a cyano group in the *para* position to the triazene moiety should give rise to the strongest mesomeric effect, followed by one carboxy substituent in the *para* position. The mesomeric effect of the latter is roughly comparable with the inductive effect of two carboxy substituents in the *meta* position. A smaller inductive effect is expected for a single carboxy substituent in the *meta* position. It is worthwhile noting that the chemical shift differences of the two CH_3 end groups in the N^3—ethyl substituents, as recorded at low temperatures, reflect this sequence precisely. The chemical shift differences $\Delta\nu$ [Hz], which reflect the *cis*- and *trans*-positions of the alkyl substituents R′ with respect to the aniline moiety in the

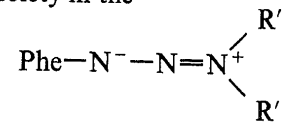

group, are included in the last column of Table 1. They are largest for the 4-cyano-substituted derivative **6**, and smallest for the 3-carboxy derivative **1**.

With regard to the steric influence of the two alkyl-substituents on N^3, the largest effect is expected for two isopropyl groups, as a consequence of their bulkiness. Among the substituents included in Table 1, the smallest steric effects will be caused by two ethyl groups.

As an alternative explanation, the possibility that internal rotation might be acid catalysed by protonation at N^3 should be discussed. Differences between the investigated compounds would then be due to differences in the basicity of N^3. Although compounds **1–5** do contain a carboxylic acid group that might act as a source of protons, this is not the case for the *p*-cyano derivative **6**. Traces of acid introduced together with the residual water present in the solvents, CD_3OD and C_6D_{12}, respectively, would have to be invoked. More important, triazene compounds are known[2,3] to be unstable in acid, where they are rapidly decomposed subsequent to protonation. In contrast, no signs of decomposition have been found in our NMR experiments, and therefore this interpretation can be excluded.

Hindered rotation

The coalescence temperatures shown in Table 2 will now be discussed in sequence. First, we consider the series of compounds **1** → **4** → **5** → **6** (cf. Table 1), in which the electron-withdrawing character of the substituents on the aromatic ring is increased, with the N^3 substituents held constant. The coalescence temperatures increase in the same sequence as the mesomeric effect is enhanced and the formation of the 1,3-dipolar structure is favoured.

Steric effects are evident when considering the series **1** → **2** → **3**. Replacing two ethyl groups by two *n*-propyl chains increases the coalescence temperature by 8 °C as a consequence of the higher mass of the $—N^3(R_4)_2$ rotor. Exchanging the *n*-propyl substituents for the bulkier *i*-C_3H_7 groups results in a further increase of T_c by 11 °C, which may be due to either steric or electron-donation effects.

The free energies of activation, $\Delta G^{\neq}$, are also strongly influenced by the mesomeric effect. Generally, $\Delta G^{\neq}$ is found to increase with T_c. (The triazene derivative **3**, with a comparatively low $\Delta G^{\neq}$ value, represents the only exception from the monotonic increase of $\Delta G^{\neq}$ with T_c.) The values derived for $\Delta H^{\neq}$ and $\Delta S^{\neq}$ should

only be discussed in a qualitative manner, in view of the large error bars. Comparable values for 1-aryl-3,3-dialkyltriazenes have been published elsewhere.[6]

The observed dependence of the internal rotation rate constant, k, on the substituents on the phenyl ring can be represented by a Hammett type equation

$$\log k/s^{-1} = \log k_0/s^{-1} + \rho\sigma \qquad (11)$$

where k_0 is the rate constant for the reference compound without substituents at the aromatic ring and σ is the Hammett substituent parameter. A Hammett plot, including data from some additional triazene derivatives, is shown in Fig. 6 for a temperature of 273 K. Linear regression of the data yields $\log k_0/s^{-1} = 2.38 \pm 0.08$ and $\rho = -1.95 \pm 0.21$. This value of ρ is in excellent agreement with published data,[6] where values of around -2 have been reported for similar systems. According to Sieh *et al.*,[3] the negative sign and the observed magnitude of ρ suggest that the rotational barrier is due to π-overlap between the amino and azo nitrogens, which is lost when the dialkylamino group is rotated by 90°. Thus, the observed Hammett correlation provides further support for our interpretation in terms of the 1,3-dipolar structure.

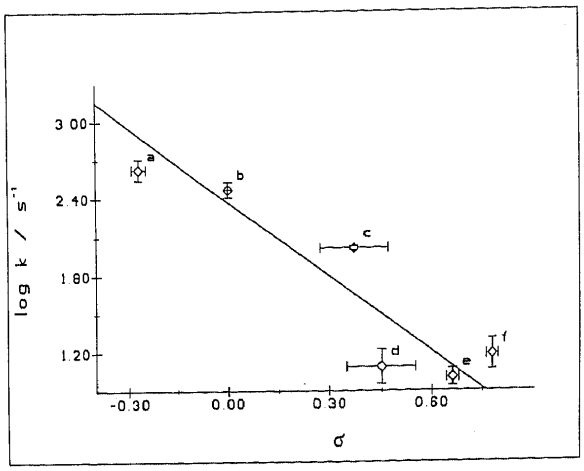

Figure 6. Hammett plot of the rate constant k of internal rotation at $T = 273$ K. The effect of substituents on the aromatic ring is represented by standard Hammett parameters, σ. Triazene derivatives used for the plot are: (a) 1-(*p*-methoxyphenyl)-3,3-diethyltriazene; (b) 1-phenyl-3,3-diethyltriazene; (c) 1-(*m*-carboxyphenyl)-3,3-diethyltriazene (compound **1**); (d) 1-(*p*-carboxyphenyl)-3,3-diethyltriazene (compound **5**); (e) 1-(*p*-cyanophenyl)-3,3-diethyltriazene (compound **6**); (f) 1-*p*-nitrophenyl)-3,3-diethyltriazene.

Thermal decomposition

The above-mentioned trends are also supported by the DSC measurements. The decomposition temperature (temperatures T_{max} of maximum heat flow in the DSC measurements) increase with the electron-withdrawing effect of the substituents at the aromatic ring. As a consequence, triazene **6**, with the cyano group in *para* position, shows no decomposition below 280°C. The bulkiness of the dialkyl groups at N^3 appears to be of lesser importance, as the decomposition temperatures increase only by smaller increments.

It is interesting to compare the activation energies determined for the thermal decomposition of the triazenes (typically, 240–280 kJ mol^{-1}, cf. Table 3) with the corresponding values determined[10] for a variety of aryl-alkyl-azo compounds (typically, 120–140 kJ mol^{-1}). The E_a values observed for the triazenes are significantly higher, i.e. by a factor of two. Quantification of this phenomenon is currently in progress. Explanations could include the effects of hydrogen bonds formed by the carboxy or dicarboxy groups, and the possible importance of decarboxylation reactions.

^{15}N chemical shift data

The results obtained in this study are helpful in interpreting ^{15}N chemical shielding data of triazenes published elsewhere.[11,12] A series of 1-phenyl-3,3-dialkyl triazenes has been investigated; the relevant chemical shift values are given in Table 4. We have

Table 4. ^{15}N chemical shift values[a] for substituted[b] triazenes, from Wilman[11]

R_1	R_2	R_4	$R_{4'}$	$\delta(N^1)$ (ppm)	$\delta(N^2)$ (ppm)	$\delta(N^3)$ (ppm)
H	OCH_3	CH_3	CH_3	−22.80	66.35	−228.16
H	CH_3	CH_3	CH_3	−23.68	68.12	−226.29
H	H	CH_3	CH_3	−25.49	69.22	−224.23
H	Cl	CH_3	CH_3	−30.99	69.25	−221.83
H	COOH	CH_3	CH_3	−32.41	71.28	−217.67
H	CF_3	CH_3	CH_3	−34.41	71.62	−217.23
H	NO_2	CH_3	CH_3	−39.26	73.01	−210.64
COOH	H	CH_3	CH_3	−30.15	69.75	−221.48
$(CF_3)_2$[c]	H	CH_3	CH_3	−42.01	71.38	−213.30
H	$CONH_2$	CH_3	CH_3	−30.77	70.55	−220.15
H	$CONH_2$	C_2H_5	C_2H_5	−33.58	68.05	−195.44
H	$CONH_2$	*i*-C_3H_7	*i*-C_3H_7	−35.72	66.62	−180.01
H	$CONH_2$	CH_3	C_2H_5	−31.47	69.53	−207.14
H	$CONH_2$	CH_3	*i*-C_3H_7	−32.87	68.81	−198.26
H	$CONH_2$	CH_3	$(CH_2)_2CH_3$	−31.32	70.13	−208.24
H	$CONH_2$	CH_3	$(CH_2)_{11}CH_3$	−31.70	70.02	−209.14

[a] Chemical shifts are given in ppm relative to nitromethane, CH_3NO_2.
[b] For the numbering of substituents, refer to Scheme 2.
[c] $R_1 = CF_3$; $R_3 = CF_3$.

maintained the numbering of the substituents introduced in Scheme 2; in cases where the two alkyl substituents at N^3 differ, they have been labelled R_4 and $R_{4'}$, respectively.

Before going into details, we comment on the range of chemical shifts covered by the data in Table 4. Nitrogen atom N^3 is less shielded than expected for an aliphatic amine [e.g. $\delta = -331.7$ ppm for $N(C_2H_5)_3$ in CH_3OH solution.[13]] At the same time, nitrogen N^1 is more shielded than expected for an N=N double bond [e.g. $\delta = +129$ ppm for *trans*-azobenzene in $CDCl_3$; Webb *et al.*[13]]. These facts are compatible with the involvement of the 1,3-dipolar resonance structure **II** shown in Scheme 1, as has been pointed out by other workers.[12]

The influence of substituents in *para*-position (R_2) and in *meta*-position (R_1) on the phenyl ring is now discussed. The changes agree with our expectations from the NMR and DSC measurements. Introduction of an electron-withdrawing substituent R_2 promotes the development of the 1,3-dipolar structure, with the consequence that N^1 is more shielded and N^3 is deshielded compared with $R_2 = H$ (cf. Table 4). In contrast, the dipolar charge distribution is reduced by electron-donating substituents in the *para*-position ($R_2 = -OCH_3$ or CH_3, respectively), and the chemical shift values of N^1 and N^3 are altered in the opposite direction (Table 4).

The effect of the *meta*-substituents R_1 generally has the same sign but is considerably smaller than that of *para*-substituents because the negative charge from N^1 is less well delocalized over the aromatic ring for *meta* substitution.

Additional data are provided by Wilman[11] for a series of compounds in which the substituent $R_2 = -CONH_2$ is held constant, and one or both alkyl substituents R_4 at the N^3 position is varied (Table 4). Generally, substitution by longer or bulkier alkyl substituents increases the shielding of N^1 and decreases the shielding of N^3. In the light of this argument, this implies that formation of the 1,3-dipolar structure is again promoted by heavier alkyl substitution. This might be interpreted either as an effect of electron donation, or more likely as a secondary effect, as heavier R_4 substituents decrease the rate of the internal rotation around the N^2-N^3 bond.

Whatever the interpretation, the chemical shift changes observed on variation of the substituent R_4 are fully consistent with our present data on the hindered rotation and thermal decomposition of compounds **1–3**. The coalescence temperature, activation parameters, and decomposition temperatures were all observed to increase as the substituent R_4 was varied in the sequence $C_2H_5 \rightarrow n\text{-}C_3H_7 \rightarrow i\text{-}C_3H_7$.

The variation of the chemical shift values for the central nitrogen atom N^2 are more complex to interpret. No changes can be predicted from the simple resonance structures of Scheme 1. Inspection of Table 4 suggests that two opposing effects may be active for $\delta(N^2)$, i.e. the formation of the dipolar resonance structure and steric effects. Thus in the series of substitutions $R_4{=}CH_3 \rightarrow C_2H_5 \rightarrow i\text{-}C_3H_7$, the shielding of N^3 decreases while the shielding of N^2 increases. A similar trend has been reported for substituted hydrazines $(CH_3)_2-N^2-N^3-(R_4R_{4'})$, where the chemical shifts of N^3 and N^2 exhibited opposite changes on variation of the substituents R_4 and $R_{4'}$.[14]

CONCLUSIONS

In this study information on the structure of phenyldialkyltriazenes,

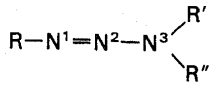

has been obtained by three independent techniques. Thermoanalytical characterization of the thermal decomposition, NMR studies of the exchange of substituents R′ and R″, and ^{15}N chemical shift values from published data[11] all indicate that internal rotation around the N^2-N^3 bond is hindered, and that the electronic structure contains a contribution from a 1,3-dipolar resonance structure

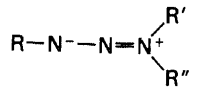

The importance of this dipolar structure is increased by the introduction of electron-withdrawing substituents on the phenyl ring, R, due to mesomeric effects. Introduction of cyano or carboxy groups in the 4-position with respect to N^1 results in the strongest increase in the N^2-N^3 double bond character. As expected, the presence of one or two —COOH groups in 3-position has much weaker effects. In addition, the charge separation is also influenced by the nature of the substituents, R′ and R″, at the amino nitrogen N^3. Introduction of longer or bulkier alkyl substituents also favours the development of the 1,3-dipolar structure; here the consequences of the increased mass on the internal rotation, as well as steric effects, are important.

Thermal decomposition temperatures increase from 113 °C to greater than 150 °C in the sequence of compounds **1** → **5** in which the N^2-N^3 double bond character increases. No decomposition was detected up to the sublimation point at 280 °C for the 4-cyano derivative **6**. Activation energies of decomposition increasing from 240 to 280 kJ mol^{-1} have been determined.

The kinetic parameters of hindered internal rotation around the N^2-N^3 bond, determined from NMR line shape and coalescence measurements, follow the same trends. The free energies of activation, $\Delta G^{\neq}$, increase from 57 to 63 kJ mol^{-1} in the sequence of triazene derivatives **1** → **6**.

^{15}N chemical shift values from references 11–14 are in agreement with this interpretation. The shielding of nitrogen atom N^3 is smaller than that found in aliphatic amines, confirming the presence of a partial N^2-N^3 double bond. On the other hand, the nitrogen nucleus N^1 is more shielded than, e.g., the nuclei in, *trans*-azobenzene, as a consequence of the negative charge at this atom. Changes in the chemical shift values have been followed as a function of substitutions, both on the aromatic ring and at the amine nitrogen. The variations expected as a consequence of both mesomeric and steric effects have been fully confirmed.

Acknowledgements

We are indebted to J. Reiner for recording the NMR spectra, and to SL Computing for the development of data reduction software.

Financial support of this work by the Deutsche Forschungsgemeinschaft (SFB 213) is gratefully acknowledged.

REFERENCES

1. O. Dimroth, *Ber. Dtsch. Chem. Ges.* **36**, 909 (1903).
2. D. M. Sieh and C. J. Michejda, *J. Am. Chem. Soc.* **103**, 442 (1981).
3. D. M. Sieh, D. J. Wilbur and C. J. Michejda, *J. Am. Chem. Soc.* **102**, 3883 (1980).
4. M. Julliard, M. Scelles and A. Guillemonat, *Tetrahedron Lett.* 375 (1977).
5. A. Gescher, J. A. Hickmann, R. J. Simmonds, M. F. G. Stevens and K. Vaughan, *Biochem. Pharmacol.* **30**, 89 (1981).
6. M. H. Akthar, R. S. McDaniel, M. Feser and A. C. Oehlschlager, *Tetrahedron* **24**, 3899 (1968).
7. R. J. LeBlanc and K. Vaughan, *Can. J. Chem.* **50**, 2544 (1972).
8. J. E. Anderson and J. M. Lehn, *J. Am. Chem. Soc.* **89**, 81 (1967).
9. O. Nuyken and R. Weidner, *Adv. Polym. Sci.* **73/74**, 145 (1986).
10. O. Nuyken, J. Gerum and R. Steinhausen, *Makromol. Chem.* **180**, 1497 (1979).
11. D. E. V. Wilman, *Magn. Reson. Chem.* **28**, 729 (1990).
12. T. Axenrod, P. Mangiaracina and P. S. Pregosin, *Helv. Chim. Acta* **59**, 1655 (1976).
13. G. A. Webb, L. Stefaniak and M. Witanowski, *Annual Reports on NMR Spectroscopy*, edited by G. A. Webb, Vol. 18, pp. 247 and 563, Academic Press, London (1986).
14. G. A. Webb, L. Stefaniak and M. Witanowski, *Annual Reports on NMR Spectroscopy*, edited by G. A. Webb, Vol. 116, p. 214, Academic Press, London (1981).

APPENDIX

Characterization of reaction productions 1–6 (cf. Experimental Section)

Product 1. Melting point, 105 °C; decomposition, 113 °C.
^{1}H NMR in DMSO-d_6 at room temperature: $\delta = 1.25$ ppm (t, 6H); 3.80 ppm (q, 4H); 7.40–8.00 ppm (m, 4H); 12.95 ppm (s, 1H). IR in KBr pellet: ν(C=O) = 1686 cm^{-1}.
UV in DMSO: $\lambda_{max} = 292$ nm; $\varepsilon = 15900$ l mol^{-1} cm^{-1}.
Elemental analysis: $C_{11}H_{15}N_3O_2$ ($M_r = 221.26$). Calc. C 59.71%, H 6.83%, N 18.99%; found C 59.93%, H 6.53%, N 18.53%.

Product 2. Melting point, 84 °C; decomposition, 128 °C.
^{1}H NMR in DMSO-d_6: $\delta = 0.80$–0.95 ppm (t, 6H); 1.55–1.75 ppm (m, 4H); 3.55–3.75 ppm (t, 4H); 7.3–7.9 ppm (m, 4H); 12.7–13.1 (s, 1H).
IR in KBr pellet: ν(C=O) = 1690 cm^{-1}.
UV in DMSO: $\lambda_{max} = 293$ nm; $\varepsilon = 14800$ l mol^{-1} cm^{-1}.
Elemental analysis: $C_{13}H_{19}N_3O_3$ ($M_r = 249.26$). Calc. C 62.64%, H 7.67%, N 16.86%; found C 62.57%, H 7.59%, N 16.52%.

Product 3. Melting point, 129 °C; decomposition, 136 °C.
^{1}H NMR in DMSO-d_6: $\delta = 1.1$–1.6 ppm (d, 12H); 3.95–4.25 and 5.05–5.3 ppm (m, 2H); 7.35–7.9 ppm (m, 4H); 12.75–13.0 ppm (s, 1H).
IR in KBr pellet: ν(C=O) = 1682 cm^{-1}.
UV in DMSO: $\lambda_{max} = 288$ nm; $\varepsilon = 15000$ l mol^{-1} cm^{-1}.
Elemental analysis: $C_{13}H_{19}N_3O_2$ ($M_r = 249.26$). Calc. C 62.63%, H 7.68%, N 16.85%; found C 62.31%, H 7.71%, N 16.57%.

Product 4. Decomposition at 151 °C, before melting.
^{1}H NMR in DMSO-d_6: $\delta = 1.15$ ppm (t, 6H); 3.75 ppm (q, 4H); 8.0–8.2 ppm (m, 3H); 13.0–13.3 ppm (s, 2H).
IR in KBr pellet: ν(C=O) = 1697 and 1686 cm^{-1}.
UV in DMSO: $\lambda_{max} = 300$ nm; $\varepsilon = 17400$ l mol^{-1} cm^{-1}.
Elemental analysis: $C_{12}H_{15}N_3O_4$ ($M_r = 265.27$). Calc. C 54.33%, H 5.70%, N 15.84%; found C 54.17%, H 5.84%, N 15.10%.

Product 5. Decomposition above 148 °C, before melting.
^{1}H NMR in DMSO-d_6: $\delta = 1.0$–1.4 ppm (m, 6H); 3.65–3.90 ppm (m, 4H); 7.25–8.0 ppm (m, 4H); 12.6–12.75 ppm (s, 1H).
IR in KBr: ν(C=O) = 1676 cm^{-1}.
UV in DMSO: $\lambda_{max} = 330$ nm; $\varepsilon = 20500$ l mol^{-1} cm^{-1}.
Elemental analysis: $C_{11}H_{15}N_3O_2$ ($M_r = 221.26$). Calc. C 59.71%, H 6.83%, N 18.99%; found C 59.59%, H 6.85%, N 18.23%.

Product 6. Sublimation starting at 280 °C, without decomposition.
^{1}H NMR in DMSO-d_6: $\delta = 1.05$–1.45 ppm (dt, 6H); 3.65–3.95 ppm (m, 4H); 7.35–7.85 ppm (m, 4H).
IR in KBr pellet: ν(C≡N) = 2216 cm^{-1}.
UV in DMSO: $\lambda_{max} = 334$ nm; $\varepsilon = 26300$ l mol^{-1} cm^{-1}.
Elemental analysis: $C_{11}H_{14}N_4$ ($M_r = 202.26$). Calc. C 65.32%, H 6.98%, N 27.70%; found C 65.28%, H 6.93%, N 27.35%.